Oxidation of Metals, Vol. 58, Nos. 5/6, December 2002 (© 2002)

Influence of Sulfur, Platinum, and Hafnium on the Oxidation Behavior of CVD NiAl Bond Coatings

J. A. Haynes,* B. A. Pint,* K. L. More,* Y. Zhang,*† and I. G. Wright*

Received January 8, 2002; revised April 22, 2002

The influences of S, Pt, and Hf on the oxidation behavior of chemical vapor deposition (CVD) NiAl bond coatings on high-S and low-S superalloys were investigated. Cyclic and isothermal-oxidation testing at 1150°C revealed that alumina-scale adherence to NiAl coatings was very sensitive to substrate S impurities. Scale spallation, as well as the growth of voids at the oxide–metal interface, increased as S increased. However, Pt-modified coatings were not sensitive to S, and did not form voids at the oxide–metal interface. Transmission-electron microscopy (TEM) revealed that alumina scales formed on (Ni,Pt)Al had Hf ions (from the superalloy) segregated to grain boundaries, whereas Hf was not detected in the alumina scale formed on NiAl coatings. Results suggested that the detrimental influence of S on scale adherence to NiAl is primarily related to void growth, which is eliminated or significantly reduced in Pt-modified coatings. A simple model relating void growth to excess vacancies and sulfur segregation is proposed.

KEY WORDS: aluminide bond coating; sulfur; platinum; hafnium; voids.

INTRODUCTION

Thermal-barrier coating (TBC) systems, which consist of a thermally insulating ceramic top coat overlying an oxidation-resistant metallic bond coat, protect hot-section components in gas-turbine engines. The bond-coat surface oxidizes to form a thin, protective Al_2O_3 scale along the metal ceramic interface.[1–3] Spallation of state-of-the-art TBCs is often associated

*Oak Ridge National Laboratory, Oak Ridge, Tennessee 37831-6063.
†Tennessee Technological University, Cookeville, Tennessee.

0030-770X/02/1200-0000/0 © 2002 Plenum Publishing Corporation

Proof

with failure at or near the brittle Al_2O_3 scale.[1–5] Tremendous interest is currently focused on methods of enhancing oxide-scale adherence, in order to enable development of TBCs with improved reliability and durability.[4,6]

As turbine-inlet temperatures continue to rise, it is likely that diffusion-aluminide bond coats will receive increasing use because of their excellent oxidation resistance and low coefficient of thermal expansion relative to Ni–Co–Cr–Al-based bond–coat alloys.[7] However, a current barrier to design of advanced bond coats is the limited understanding of the mechanisms controlling oxide-scale adherence. For example, although Pt has been added to diffusion-aluminide coatings and laboratory alloys for over three decades to improve oxidation performance,[8–12] the mechanisms by which Pt improves Al_2O_3 scale adherence are still not clear.[13–15]

It is generally agreed that the adherence of Al_2O_3 scales is substantially degraded by the presence of substrate S impurities, since desulfurizing significantly improves oxide adherence.[16–19] It is also well known that the detrimental effects of S can be overcome by proper addition of reactive elements, such as Zr, Y, and Hf to the alloy.[20–22] Most superalloys contain small amounts of reactive elements, which may eventually diffuse through the bond coat into the oxide scale.[23] The relative influences of sulfur, platinum, and reactive elements on the growth and adherence of oxide scales on aluminide-bond coats have not yet been clearly defined.

The objective of this study was to investigate the influences of Pt alloying additions and variations in substrate S impurities on alumina-scale growth and adherence to aluminide-bond coatings on single-crystal superalloy substrates. A secondary objective was to observe the behavior of nominal amounts of Hf present in all of the single-crystal superalloy substrates. The goal was to advance the mechanistic understanding of S, Pt, and reactive-element effects (REE) in order to support improved design and modeling of advanced bond coatings.

EXPERIMENTAL PROCEDURES

Two versions (standard and melt-desulfurized) of Y-free single-crystal René N5 superalloy (PCC Airfoils, Cleveland, OH) were used as coating substrates. The bulk alloy compositions were determined by inductively coupled plasma (ICP) analysis (Table I). The bulk S content of the standard alloy, referred to hereafter as high-S (HS), was measured at ~7.0 ppma (~3.6 ppmw) by glow-discharge mass spectroscopy (GDMS) using a VG 9000 glow-discharge mass spectrometer (GDMS) (VG Elemental, Winsford, UK). The S content of the melt-desulfurized version of the alloy, referred to hereafter as low-S (LS), was measured at 1.0 ppma (0.8 ppmw) by GDMS. The two alloys were consecutively analyzed using the same GDMS

Table I. Chemical Compositions of Superalloy Substrates (at.%)

Element	HS René N5	LS René N5
Ni	64.8	64.7
Cr	8.1	8.1
Co	7.4	7.5
Al	13.8	13.5
Ta	2.0	2.1
W	1.4	1.7
Mo	0.8	0.9
Re	0.9	1.0
Ti	ND	0.01
Si	0.11	0.09
Fe	0.35	0.09
P (ppma)	57	78
N (ppma)	25	26
B (ppma)	274	278
O (ppma)	96	68
C (ppma)[a]	4846	4930
Hf (ppma)[a]	570	670
Y (ppma)[a]	3	3
Zr (ppma)[a]	48	45
S (ppma)[a]	7.0	1.0

[a]Data by GDMS. All others by ICP.

unit, operator, and calibration method. Limitations of the GDMS technique have been described previously.[19]

Ultrahigh-purity (UHP) NiAl coatings were fabricated on HS and LS René N5 substrates using a low-activity CVD aluminizing[24,25] procedure designed to minimize process-related S contamination.[19] Specimen coupons ($1.8 \times 1.4 \times 0.15$ cm) were prepared for coating by grinding and polishing through 0.05 μm alumina, followed by ultrasonic cleaning in acetone and methanol. Deposition conditions are reported elsewhere.[14,19] The (Ni,Pt)Al coatings were synthesized by grit-blasting and electroplating HS and LS substrates with ~7 m of Pt (Howmet Corporation, Whitehall, MI) and then aluminizing in the same CVD reactor. The electroplated Pt in this study contained greater than 200 ppma S by GDMS sputter profiling.[14] Hereafter, coatings on the LS René N5 will be referred to as LS NiAl and LS (Ni,Pt)Al and coatings on the HS René N5 will be referred to as HS NiAl and HS (Ni,Pt)Al.

The cyclic and isothermal-oxidation behaviors of the four types of coatings, as well as selected cast NiAl and (Ni,Pt)Al reference materials, were evaluated at 1150°C. The HS and LS superalloys (with no bond coat) were cyclically tested at 1100°C in a previous study.[26] The surfaces of all coatings

were in the as-deposited condition with no postdeposition surface modifications or heat treatments prior to oxidation testing. Automated cyclic-oxidation testing of coatings was conducted by inserting specimens into a furnace at 1150°C. Each cycle consisted of a 60-min exposure in dry flowing O_2 followed by a 10-min cooling period in ambient air. Specimens were weighed and inspected after every 20 or 50 cycles.

Isothermal-oxidation tests were conducted for 100–200 hr at 1150°C in dry oxygen, flowing at 100 cm^3/min. Specimens were suspended by a Pt–Rh wire, and were rapidly inserted and removed from the hot furnace. Mass gains were measured by continuous thermogravimetry using a Cahn Instruments Model 1000 microbalance. All kinetics data were corrected for evaporation of the Pt–Rh wire.

The phase structures of the coatings and oxide scales were determined by X-ray diffraction (XRD; PAD V, Scintag, Sunnyvale, CA). The surface morphologies of the coated specimens were examined by field-emission-gun, scanning-electron microscopy (FEG–SEM; S800 and S4700 series, Hitachi Ltd., Hitachinaki-shi, Japan) equipped with X-ray energy or wavelength-dispersive spectroscopy (FEG–SEM–EDS/WDS).

Cross-section samples for transmission-electron microscopy (TEM) were prepared by initially cutting a section from the cyclically or isothermally exposed coupon. The section was then mechanically thinned using an Allied High Tech Products Inc. (Rancho Dominguez, CA) Techprep Polishing Machine (equipped with a Multiprep Micropositioning Head) to ~50 μm thick and mounted on a Be support ring for final thinning to electron transparency using the Hitachi FB-2000A focused ion-beam (FIB) system. The FIB utilizes Ga ions to selectively etch a ~20 × 20-μm thin section from the surface of the specimen for TEM imaging. This uniformly thin "window" of material (<0.1 μm) contains all the regions of interest for subsequent TEM/STEM analysis (oxide scale + bond coat).[27] An FEI/Philips (FEI Co., Portland, OR) CM200 FEG–TEM/STEM equipped with an Oxford Super-ATW Energy-Dispersive Spectrometer (EDS) and an EMiSPEC (EMiSPEC Systems Inc., Tempe, AZ) integrated acquisition system for X-ray microanalysis was used for dark- and bright-field imaging and high-resolution elemental mapping of the full oxide scale–bond coat interfacial region.

RESULTS

Coating Phases, Microstructures, and Compositions

The CVD process results in an outward-grown layer of single-phase β-NiAl or β-(Ni,Pt)Al, with an underlying interdiffusion zone consisting of refractory metal-rich precipitates in a β matrix.[14,15,19] The coatings had a

microstructure typical of CVD aluminides, consisting of large, polygonal grains (25–150 μm diameter), with prominent surface ridges outlining each grain, as shown in Fig. 1. The coatings were columnar-grained, with each grain boundary extending across the entire thickness. The NiAl and

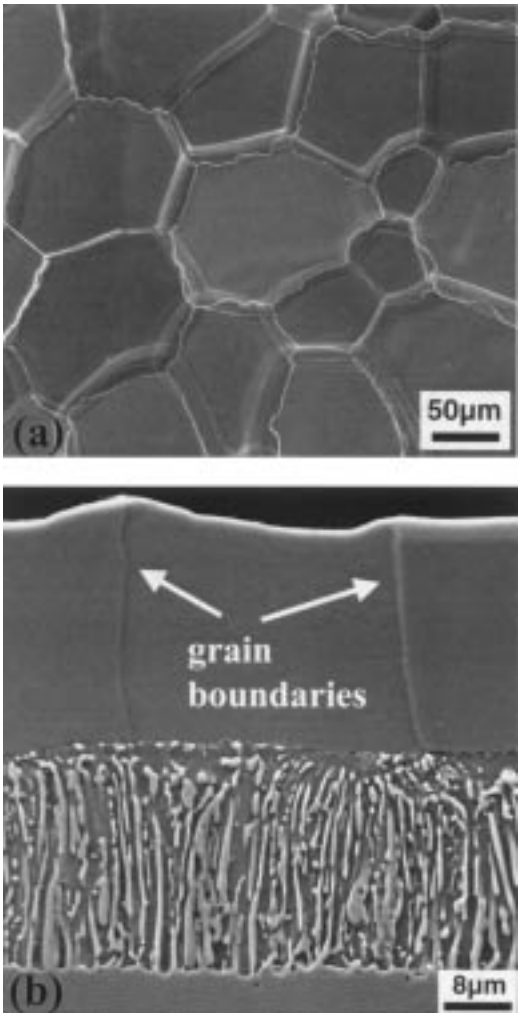

Fig. 1. Secondary-electron images of: (a) as-deposited CVD (Ni,Pt)Al coating surface and (b) polished and etched cross section of as-deposited CVD NiAl.

(Ni,Pt)Al coatings were typically ~25 and ~35 μm thick, respectively. XRD indicated a β-NiAl (B2) structure for as-deposited NiAl and (Ni,Pt)Al.

The composition at the surface of the as-deposited CVD NiAl was approximately 50 Ni, 44 Al, 4.5 Co, and 1.0 Cr (at.%; Co and Cr were from the superalloy substrate) as determined by electron-microprobe analysis of a polished cross section. The composition at the surface of the as-deposited CVD (Ni,Pt)Al coating was approximately 43.1 Ni, 45.9 Al, 6.1 Pt, 3.6 Co, and 1.0 Cr (at.%). The average Al concentrations across the NiAl and (Ni,Pt)Al coatings were 40.3 and 41.3 at.%, respectively. Detailed compositional analyses of these coatings are reported elsewhere.[14,15]

Sulfur in the as-deposited LS NiAl coatings was measured at less than 0.5 ppma by GDMS sputter profiling.[14] Sulfur in the as-deposited LS (Ni,Pt)Al was similar to that in the LS NiAl (<0.5 ppma), although there was a S peak of ~6 ppma at the gas surface of the LS (Ni,Pt)Al. Both coatings contained significant amounts of S near the original superalloy interface, as determined by GDMS sputter depth profiling, with S peaking at ~6.0 ppma in LS NiAl and >200 ppma in LS (Ni,Pt)Al.[14] There were no GDMS analyses of coatings on the HS alloy, but it was assumed that the CVD NiAl S levels were equal to or higher than those on the LS substrates.

Cyclic Oxidation of Superalloys

Figure 2 compares the cyclic oxidation behavior of HS (7.0 ppma S) and LS (1.0 ppma S) single-crystal René N5 (no bond coating) tested at 1100°C in a previous study.[26] These specimens were cut from the same batches of Y-free superalloy used as coating substrates in the present study. The HS superalloy experienced significant mass loss beginning at 30–50 cycles and continued to lose mass throughout the duration of the test (–2.4 mg/cm after 250 cycles), indicating very poor oxide-scale adherence. The LS alloy exhibited good oxide-scale adherence, with minimal evidence of mass loss (+3.3 mg/cm^2 after 1200 cycles). Additional cyclic-oxidation testing of just the LS alloy revealed good adherence at 1150°C, with indications of mass loss beginning at approximately 200 cycles and a mass change of ~0.1 mg/cm^2 after 500 cycles, likely due to spallation of surface spinel oxides.[26] Previous investigators[26,28] have suggested that the Hf/C ratio in René N5 should be considered as an important influence on oxidation behavior, since Hf is a strong carbide former (forming carbides more stable than oxides). However, in this study, both the HS and LS alloys contained nearly identical amounts of Hf and C (~600 and ~4900 ppma, respectively, by GDMS), supporting the premise that the significant differences in superalloy oxidation behavior were primarily related to S content.

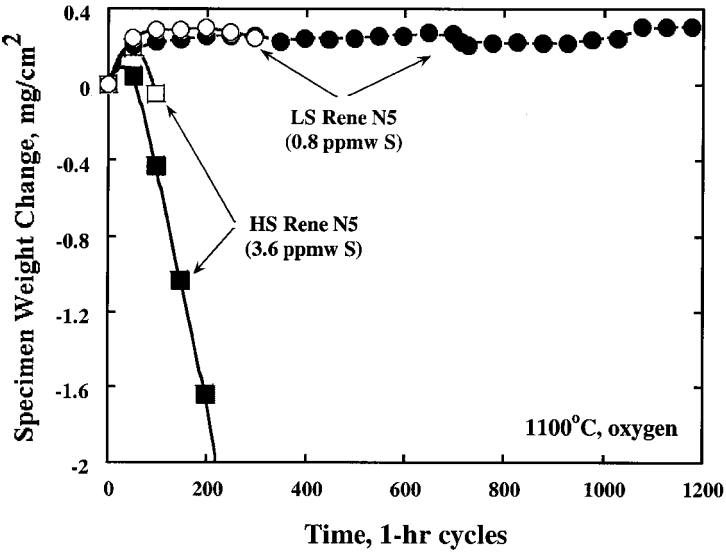

Fig. 2. Plots of specific mass change vs. number of cycles demonstrating the relative scale adherence to uncoated HS and LS Renné N5 substrates at 1100C. The same batches of Y-free superalloy were used as substrates for the NiAl and (Ni,Pt)Al coatings.

Cyclic Oxidation of NiAl Castings and Coatings

The specific mass changes measured during 1150°C cyclic-oxidation testing of NiAl coatings (on the same superalloys as those in Fig. 2) and three cast NiAl reference materials are shown in Fig. 3a. One cast material was of a near-stoichiometric composition, Ni–50.1Al (at.%) with an S content of ~3.0 ppmw (by GDMS). The second was a substoichiometric composition, Ni–40Al (at.%), with an Al concentration similar to that of the as-deposited CVD NiAl (Table I) and S content of ~6.0 ppmw (by GDMS). The third reference material was Ni–48.3Al (at.%) with 0.05 at.% Hf (S was not measured).

Both of the cast Hf-free NiAl reference materials exhibited relatively poor scale adherence (Fig. 3a). The Ni–50.1Al specimen experienced a rapid initial mass gain followed by a significant mass loss between 100 and 150 cycles. The alloy continued to spall heavily, with a total mass change of -1.7 mg/cm^2 after 500 cycles. There was even more mass loss initially from Ni–40Al, due to the higher S content and possibly as a result of more rapid void growth beneath the scales due to the lower Al content of the substrate.[29] Mass losses from Ni–40Al after 500 cycles were significantly

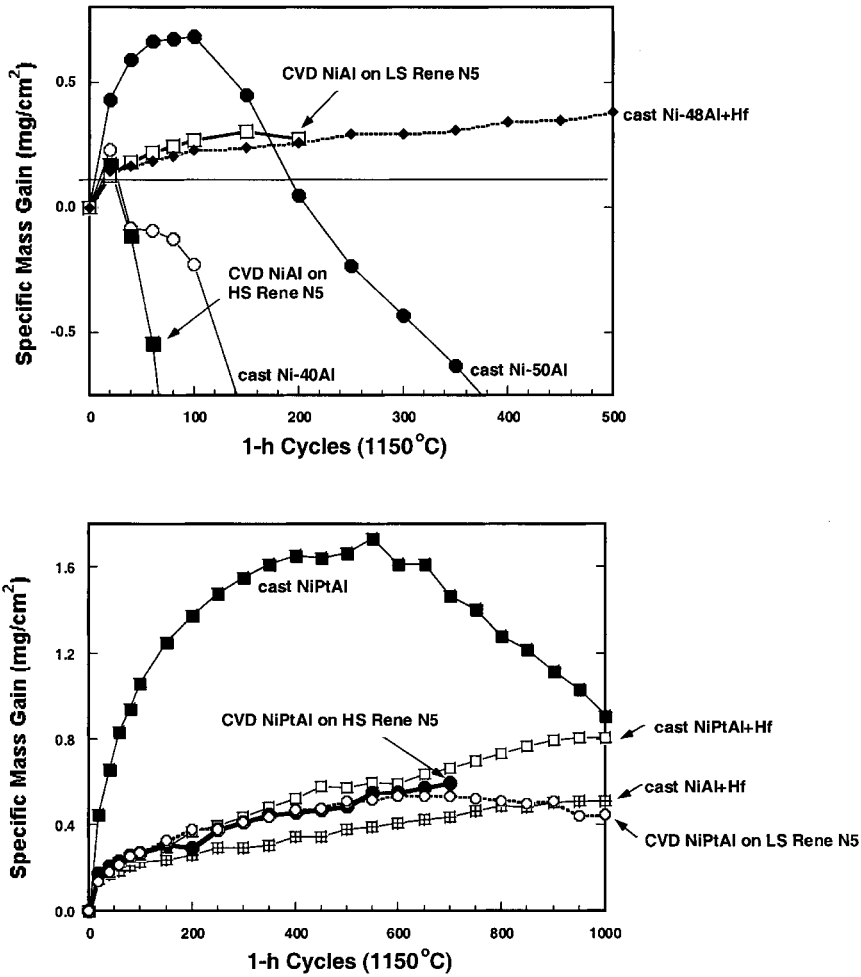

Fig. 3. Cyclic-oxidation behavior (1150°C) of (a) cast NiAl and CVD NiAl and (b) cast (Ni,Pt)Al and CVD (Ni,Pt)Al. Note the detrimental effects of S and the beneficial effects of Pt and Hf.

higher (–4.8 mg/cm^2) than Ni–50.1 Al due to the formation and spallation of faster-growing Ni-rich oxides (blue and green tinted) on the lower Al content casting.

By comparison, scale adherence to cast NiAl + Hf was excellent, with a constant mass gain and no evidence of mass loss after 1000 cycles. Mass gains at 500 and 1000 cycles were 0.38 and 0.51 mg/cm^2, respectively. As

Table II. Aluminide Coatings Exposed to Cyclic Oxidation at 1150°C

Substrate type	Coating type	Total cycles	Maximum mass gain (mg/cm^2)	Final mass change (mg/cm^2)
LS	(Ni,Pt)Al	1000	0.53	0.45
LS	(Ni,Pt)Al	800	ND[a]	ND
HS	(Ni,Pt)Al	700	0.60	0.60
LS	NiAl	200	0.30	0.27
LS	NiAl	200	0.30	0.24
HS	NiAl	100	0.17	−1.7

[a]ND: not determined; specimen was cut for metallography after 200 cycles.

can be seen from Fig. 3a, the mass gain of NiAl + Hf in the first 100 cycles was much lower than that of Ni–50.1Al due to the influence of Hf, which is known to significantly reduce Al_2O_3 growth rates[30] and improve scale adherence.[31]

Scale adherence to the CVD NiAl coating on an HS substrate was extremely poor. This higher sulfur specimen (7.0 ppma S) spalled to a mass less than that of the original within 40 cycles, with a total mass change of −1.7 mg/cm^2 after 100 cycles. The time to spallation and the rate of initial mass loss were very similar to that of the cast Ni–40Al reference material (Fig. 3a).

Scale adherence to CVD NiAl improved significantly when substrate S was reduced from ~7.0 to ~1.0 ppma (Fig. 3a).[19] The rate of mass gain of the LS CVD NiAl coatings was much lower than that of the cast NiAl, but was very similar to that of the cast NiAl + Hf. The first evidence of mass loss from LS CVD NiAl was at 200 cycles, although the total mass change was still positive (+0.28 mg/cm^2 after 200 cycles) (Fig. 3a). As reported previously,[2,14,19] SEM of the surfaces revealed that Al_2O_3 scale cracking occurred primarily along the LS NiAl grain-boundary ridges after 200 cycles, whereas scales on the aluminide grain bodies generally remained very adherent. Characterization of coating cross sections by SEM after 200 cycles revealed that the NiAl grain-boundaries had transformed to the γ'-Ni_3Al phase due to local Al depletion, whereas the coating remained β-NiAl beneath the bulk grain bodies.[13] This type of grain-boundary depletion did not occur after isothermal oxidation of the same coatings for 200 hr.[13,15] This result suggests that Al was depleted due to spallation and reformation of Al_2O_3 over the LS NiAl coating grain boundaries. There was no evidence of interfacial-void formation on LS NiAl surfaces exposed by scale spallation after 200 cycles. The cyclic oxidation behavior of a replicate LS NiAl specimen (processed in a separate CVD batch) was near identical, as indicated in Table II.

Cyclic Oxidation of (Ni,Pt)Al Castings and Coatings

The specific mass changes measured during 1150°C cyclic-oxidation testing of CVD (Ni,Pt)Al coatings (same superalloy substrates as those in Fig. 2), cast NiAl + Hf, and two cast (Ni,Pt)Al reference materials are shown in Fig. 3b. The cast (Ni,Pt)Al reference materials were Ni–2.4Pt–50.2Al (at.%) and Ni–2.4Pt–49.7Al + 0.05Hf (at.%).

The cyclic-oxidation behavior of cast (Ni,Pt)Al was clearly superior to that of cast NiAl. The cast (Ni,Pt)Al without Hf exhibited good scale adherence to approximately 500 cycles, after which a gradual, but steady, mass loss occurred. The rate of mass gain was relatively high, with total mass changes at 500 and 1000 cycles of 1.6 and 0.91 mg/cm^2, respectively. By comparison, scale adherence was much improved on the cast (Ni,Pt)Al +Hf with no evidence of mass loss and a total mass gain of only 0.81 mg/cm^2 after 1000 cycles. Again, consistent with the results of the cast NiAl (Fig. 3a and Refs. 30 and 31), the oxidation rate of Hf-doped cast (Ni,Pt)Al was significantly lower than that of Hf-free cast (Ni,Pt)Al.

Likewise, Pt-modified CVD aluminide coatings exhibited dramatic improvements in scale adherence, as compared to CVD NiAl coatings. Most significantly, scale adherence on the (Ni,Pt)Al coatings revealed no sensitivity to substrate S impurities, at least within the range of S levels in this study. Both HS and LS (Ni,Pt)Al coatings exhibited little evidence of mass loss after 700 cycles (Fig. 3b), although SEM of the coating surfaces revealed that extensive surface deformation of the CVD (Ni,Pt)Al had occurred on both specimens during cyclic oxidation (Figs. 4a and b). Characterization of the surface of a replicate LS (Ni,Pt)Al specimen (Table II) by SEM also showed no significant scale spallation after 700 cycles, although it was not possible to compare mass change for this specimen since a small section was cut for metallography after 200 cycles. Scales on coating grain-boundary ridges of all three (Ni,Pt)Al specimens were cracked but still adherent after 700 cycles (Fig. 4c and d). Localized regions of bare metal were evident on less than 1% of their surfaces after 700 cycles and no voids were visible in the exposed metal. There was evidence that an adherent alumina layer reformed after local spallation of the original scale. There were no discernable differences in the surfaces of the HS or LS (Ni,Pt)Al coatings after 700 cycles (Fig. 4). The rates of mass gain for both HS and LS CVD (Ni,Pt)Al (on superalloy substrates that contained Hf) were much lower than that of cast (Ni,Pt)Al, but were very similar to that of cast (Ni,Pt)Al + Hf. The similar rates of oxidation between cast NiAl + Hf, cast (Ni,Pt)Al + Hf, the LS NiAl, and both types of (Ni,Pt)Al coatings demonstrates the capability of small amounts of substrate Hf to reduce scale growth rates on aluminide coating surfaces at elevated temperatures.

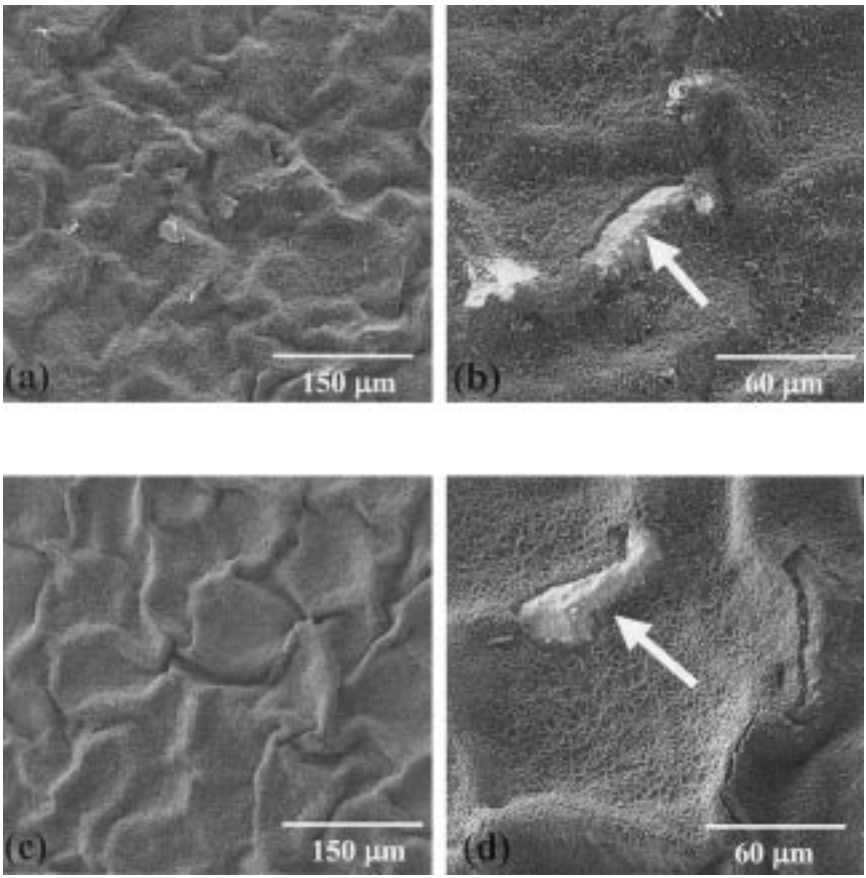

Fig. 4. Secondary-electron images of the surfaces of CVD NiPtAl bond coats after 700 1-hr cycles to 1150°C. (a) and (b) NiPtAl on low-S René N5; (c) and (d) NiPtAl on high-S René N5.

The HS (Ni,Pt)Al specimen in Fig. 3 was removed from testing for metallography after 700 cycles. The LS (Ni,Pt)Al continued to be exposed to 1000 cycles, at which time gradual decreases in mass (Table II) indicated the onset of oxide spallation (Fig 3b). The total mass change after 1000 cycles was +0.44 mg/cm^2. The LS (Ni,Pt)Al surface after 1000 cycles showed evidence of extensive oxide cracking, spallation, and scale reformation (Fig. 5a). Evidently, the scale reformed rapidly after spallation as there was still very little bare metal exposed (arrows in Fig. 5a). However, small voids (<15 μm diameter) were occasionally observed within the bare metal exposed by scale spallation after 1000 cycles (Fig. 5b). No similar voids were

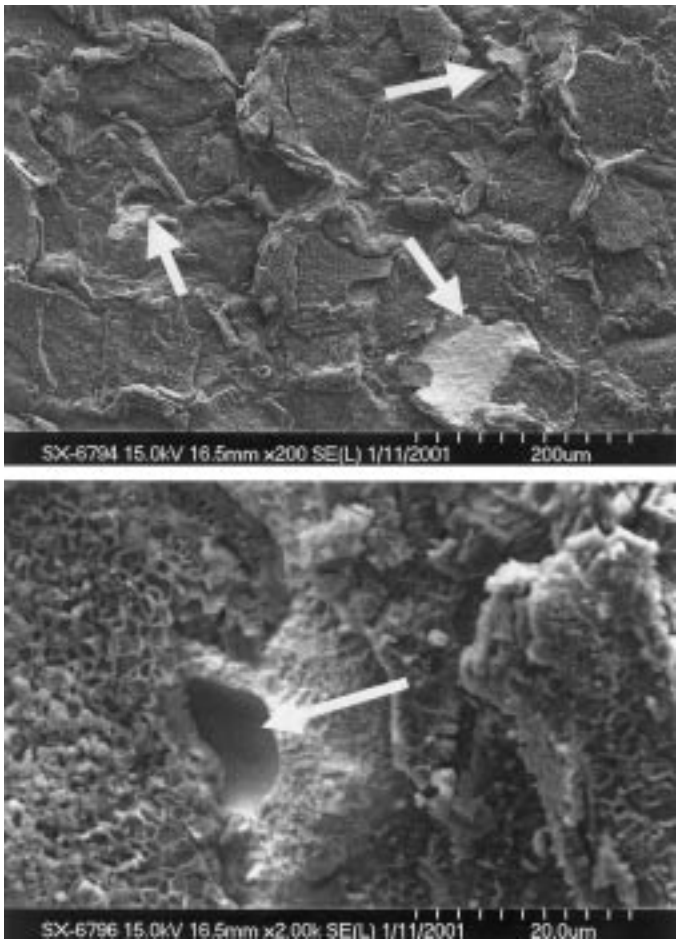

Fig. 5. SEM images of a low-S (Ni,Pt)Al coating surface after 1000 cycles to 1150C. (Top) Region with most scale spallation. Although significant surface deformation and scale cracking was observed, bare metal was observed in only a few localized areas (arrows). (Bottom) Voids (arrow) were occasionally observed within the metal exposed by scale spallation, but only after 1000 cycles.

observed when this specimen was examined by SEM after 700 and 900 cycles.

Isothermal Oxidation of CVD NiAl and (Ni,Pt)Al

The steady-state parabolic rate constants (k_p) measured by thermogravimetric analysis of cast NiAl, cast NiAl + Hf, LS CVD NiAl, LS

Table III. Parabolic Rate Constants from the First 100 hr of Isothermal Oxidation

Specimen	Temperature (°C)	Time (hr)	Parabolic constant (K_p) ($g^2/cm^4/sec$)[a]
Cast NiAl	1150	100	7.8×10^{-12}
Cast NiAl + 0.05at.% Hf	1150	100	4.8×10^{-13}
CVD NiAl on LS René N5	1150	100	8.1×10^{-14}
CVD NiAl on HS René N5	1150	100	NA[b]
CVD (Ni,Pt)Al on LS René N5	1150	100	1.4×10^{-13}
CVD (Ni,Pt)Al on HS René N5	1150	100	2.3×10^{-13}

[a] Calculated from isothermal mass gains within first 100 hr.
[b] Data lost due to software failure.

CVD (Ni,Pt)Al, and HS CVD (Ni,Pt)Al are compared in Table III. The k_p of alumina on LS CVD NiAl (~600 ppma Hf in the substrate) after 100-hr isothermal oxidation at 1150°C was much lower than that of cast NiAl and was even slightly lower than on a cast NiAl + Hf (0.05 at.% Hf) reference material.[15] This comparison supports the previous observation (Fig. 3a) that Hf from the superalloy influences the oxidation behavior of the coating at 1150°C. Although cast NiAl + Hf is typically considered to exhibit one of the slowest growing alumina scales,[30,31] in these relatively short-term oxidation tests, there may have been a higher apparent rate due to near-surface internal oxidation of Hf-rich precipitates and the initial formation of faster-growing θ-Al_2O_3. There may also have been an accelerated rate of transformation of faster-growing, metastable θ-Al_2O_3 to the slower-growing α-Al_2O_3 on the NiAl coatings due to the presence of Cr or other substrate elements in the coating.[32] The k_p of LS CVD NiAl was also measurably lower than those for CVD (Ni,Pt)Al.[15,23]

Scale adherence to LS CVD NiAl was excellent for a simple aluminide at 1150°C, although localized scale spallation was commonly observed along coating grain boundaries after 100 hr isothermal oxidation due to growth of large, faceted voids at the oxide–metal interface.[33] The number of voids increased after 200 hr. Figure 6 compares void formation on the surface of the LS NiAl to that of LS (Ni,Pt)Al after 200 hr. Voids with a range of sizes (7–30 μm diameter) formed on LS NiAl, with the overlying alumina scale apparently remaining intact at temperature and then spalling during cooling, since metal surfaces of the voids were not oxidized (Fig. 7). Most voids were on grain boundaries and there were very few voids on the LS NiAl grain surfaces.[15] In contrast, there was no scale spallation from LS (Ni,Pt)Al (Fig. 6b) after 100 or 200 hr at 1150°C and there was no evidence of void growth at the oxide–metal interface when Pt-modified coatings were examined in cross section.

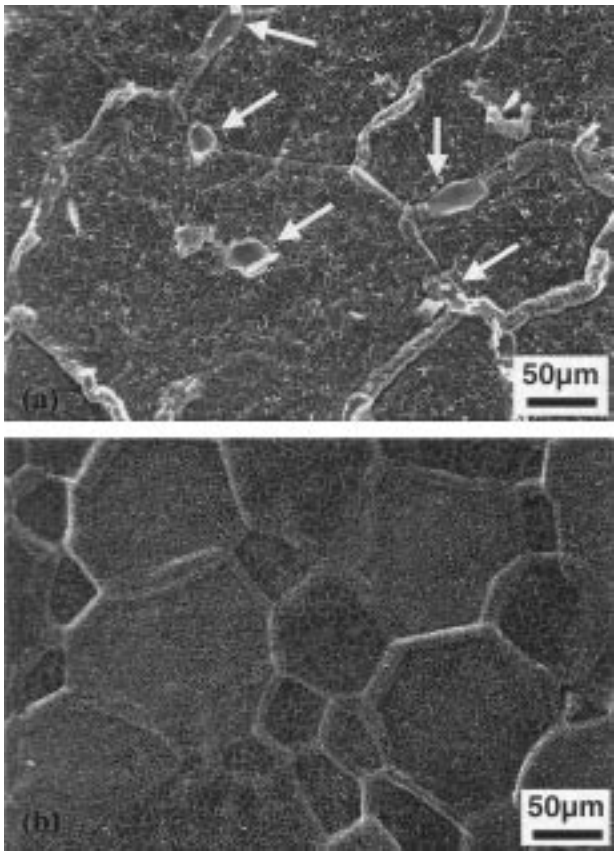

Fig. 6. SEM images of the surface of (a) LS NiAl coating and (b) LS (Ni,Pt)Al coating, after 200 hr isothermal oxidation at 1150°C. Note the presence of voids (arrows) and very localized areas of scale spallation in (a) but not (b).

Based on the trends of the cyclic-oxidation tests (Figs. 2 and 3) and the observed interfacial void growth during isothermal oxidation of the LS NiAl coatings (Fig. 6a and Fig. 7), as well as previous studies of cast intermetallics,[34–37] it was presumed that void growth on CVD NiAl might accelerate with higher concentrations of substrate S. It was also expected that an increase in substrate S would result in a higher probability of void formation on (Ni,Pt)Al. In order to test these hypotheses, specimens of HS NiAl and HS (Ni,Pt)Al were exposed to 200 hr isothermal oxidation at 1150°C.

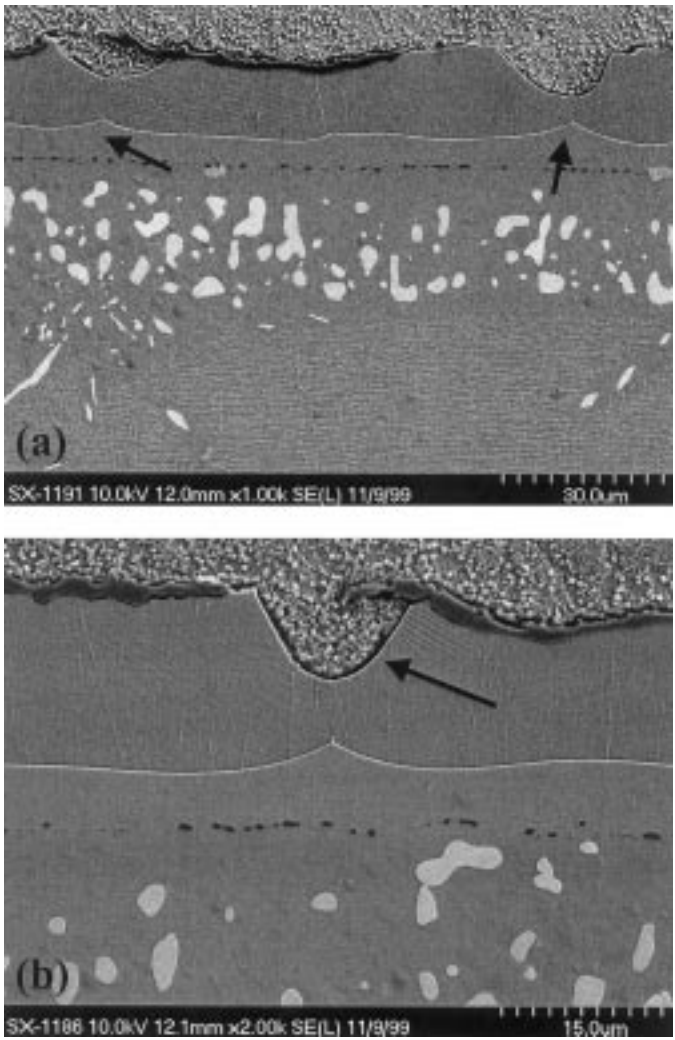

Fig. 7. SEM images of a Cu-plated LS CVD NiAl coating cross section after 200 hr isothermal oxidation at 1150°C. (a) Voids were located primarily over coating grain boundaries (arrows); (b) voids (arrow) reached depths of almost 10 μm.

Results were as expected for the HS NiAl coatings. There was a remarkable increase in the number of voids and ~40% of the scale spalled from the coating surface after 200 hr oxidation, as shown by comparison of Fig. 6a with Fig. 8. Large numbers of small-diameter, shallow voids formed

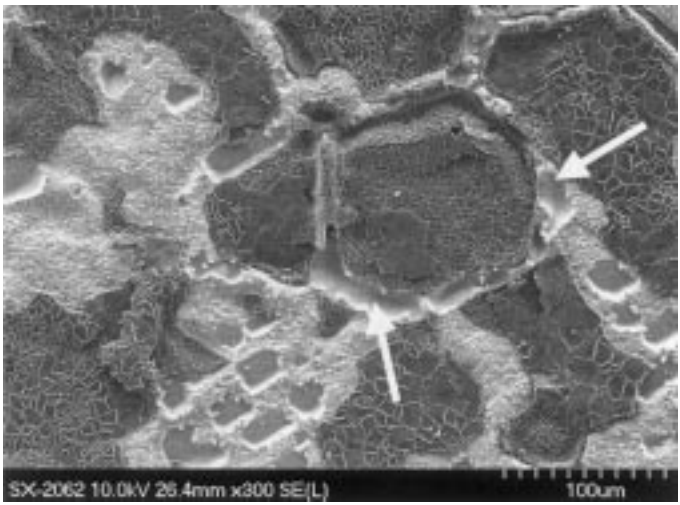

Fig. 8. SEM image of the surface of CVD NiAl on a HS substrate after 200 hr isothermal oxidation at 1150C. Note the extensive formation of small voids on the bulk grain surface and the void trenches (arrows) around the NiAl grain boundaries.

on some grain bodies, although, in many cases, adjacent grains contained no voids. Some of the grain boundaries contained very large voids (Fig. 8b). In fact, void growth was so prevalent on some grain boundaries that semicontinuous trenches formed around some grains (Fig. 8). Void diameters ranged from 4.0 to 67 μm and there was microstructural evidence that the presence and size of voids was influenced by NiAl grain orientation (i.e., not all grains or boundaries formed voids, whereas adjacent grains often contained numerous voids). However, the voids on HS NiAl (Fig. 9) were more shallow than voids of similar diameter on LS NiAl (Fig. 7). For example, the largest void on HS NiAl had a diameter of 67 μm with a depth of 7.1 μm, whereas the largest void on LS NiAl had a diameter of 30 μm with a depth of 8.5 μm. Most of the smaller voids on HS NiAl grain surfaces were ~1.0 μm in depth and many of the larger voids appeared to result from the coalescence of multiple voids.

The average ratio of void diameter to depth for HS NiAl (as measured by SEM in cross section) after 200 hr was 5.0 ± 1.8, with a maximum depth of penetration of ~7.0 μm. By comparison, the average ratio of void diameter to depth on LS NiAl after 200 hr was 3.9 ± 1.7, with a maximum depth of void penetration of ~10 μm. The relative volume of voids on both coatings could not be accurately quantified due to significant irregularities in void size, shape, aspect ratio, the apparent random formation of voids

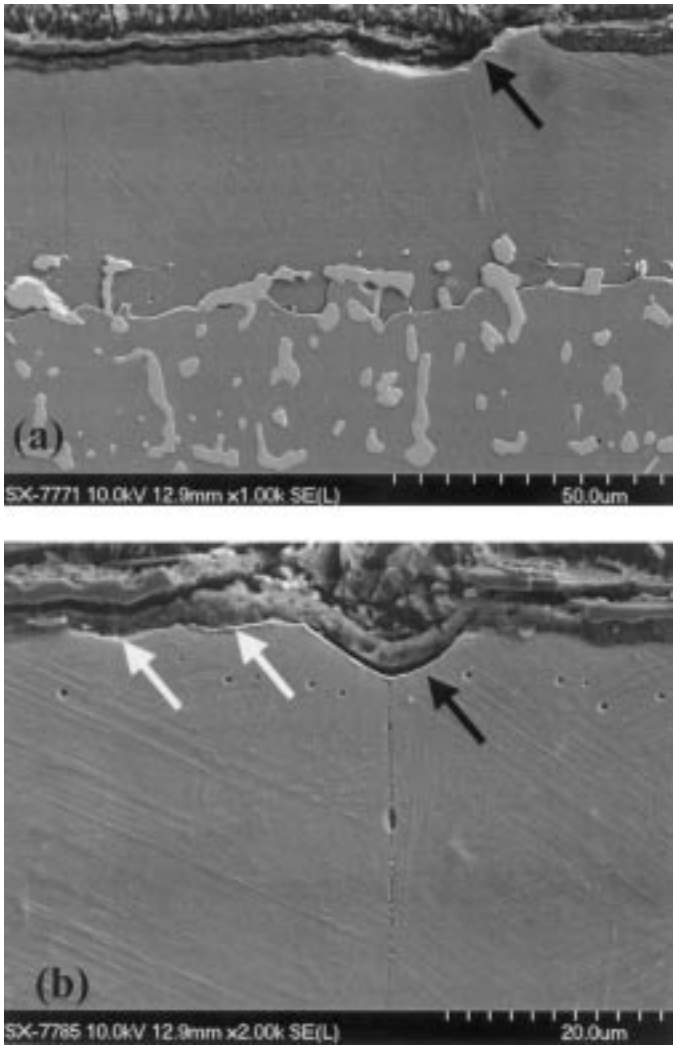

Fig. 9. SEM images of Cu-plated, etched cross sections of CVD NiAl on a HS substrate after 200 hr isothermal oxidation at 1150°C. (a) Typical large-diameter, shallow void over a coating grain boundary; (b) void over grain boundary with several adjacent, smaller voids on grain body (white arrows). The thin layer of darker-contrast material adjacent to the coating surface is epoxy that leached below the Cu plating.

(independent of grain orientation), and the difficulty of effectively imaging and measuring the very shallow voids. Similar difficulties in measuring void volume on aluminide coatings were encountered by other investigators.[38] Nevertheless, although there were many more voids on HS NiAl, the total volume of voids on HS NiAl did not appear to be dramatically different than those on LS NiAl.

In vivid contrast to the response of the NiAl coatings, increased substrate S had little effect on scale adherence to Pt-modified coatings. There was no scale spallation from HS (Ni,Pt)Al after 200 hr (Fig. 10), although the steady-state, isothermal-oxidation rate of HS (Ni,Pt)Al at 1150°C was slightly higher than that of LS (Ni,Pt)Al (Table III). There were slight differences in the alumina scale microstructure of HS and LS (Ni,Pt)Al. On HS (Ni,Pt)Al, a very thin, featureless overlayer of alumina (Al and O by EDS) was intermittently present over the underlying Al_2O_3 scale, which contained the typical Al_2O_3 surface ridges or the "lacy structure" as described by Doychak[39] (Fig 10). The thin, amorphous-appearing surface layer of Al_2O_3 was cracked, often appeared integral to the scale on the grain-boundary ridge and, in some cases, contained a few ridges. There was no cracking in the underlying ridged alumina layer. This surface layer may be the remnant of transient oxides formed during the initial stages of oxide formation, or it

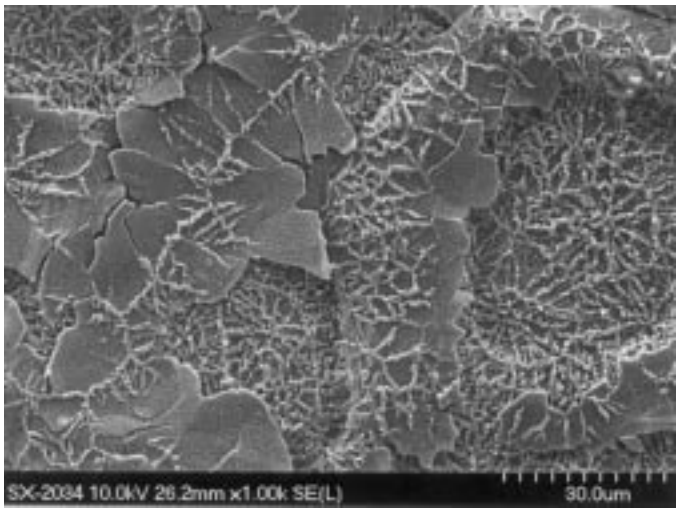

Fig. 10. Secondary-electron images of the surface of a CVD (Ni,Pt)Al on a HS substrate after 200 hr isothermal oxidation at 1150°C. No scale spallation occurred. Thin plates of alumina had apparently flaked off some surfaces, with underlying intact scale beneath.

may be a layer that detached during the early stages of scale growth. This thin overlayer was not observed on LS (Ni,Pt)Al (Fig. 6b).

No voids were detected along the oxide–metal interface by FEG–SEM analysis of metallographic cross sections of HS or LS (Ni,Pt)Al after 200 hr at 1150°C. However, both HS and LS (Ni,Pt)Al coatings contained large internal voids along the coating–superalloy interface after isothermal oxidation, as reported previously,[15] whereas the NiAl coatings did not. Further, internal voids of this type were not observed in (Ni,Pt)Al coatings after cyclic oxidation at 1150°C, in agreement with the results of Tolpygo and Clarke,[40] who postulated that the internal voids after isothermal oxidation were the result of volume contractions due to gradual phase transformation of the β-NiAl coating to γ-Ni_3Al due to Al depletion.

Characterization of Alumina Scales

The microstructures and microchemistries of the Al_2O_3 scales formed during 100 hr isothermal oxidation of LS NiAl and LS (Ni,Pt)Al were analyzed using fine-probe STEM (Figs. 11a and b). The scale on NiAl was thinner than that on (Ni,Pt)Al, in agreement with the measured differences in oxidation kinetics (Table III).

The α-Al_2O_3 scale on LS NiAl appeared to be a single-grain thick, ranging from 0.4–1.5 μm (average ~1.1 μm with a grain diameter of >2.0 μm) and contained numerous small (<100 nm) discrete, internal voids throughout most of its thickness (Fig. 11a). The 100 nm of alumina nearest the metal–oxide interface appeared to be free of voids. The porous outer region may have formed as a metastable phase, such as θ-Al_2O_3 or γ-Al_2O_3, and then transformed to stable α-Al_2O_3 polymorph, resulting in formation of voids[41] to accommodate the 14.3% volume reduction during the θ-α transformation.[42] The very thin, dense layer at the interface possibly formed as α-Al_2O_3. Some of the internal voids may be the result of encapsulation of perturbation voids that formed due to irregularities at the metal–oxide interface.[43] No voids were observed at the oxide–metal interface of the thin foils analyzed in this study, although interfacial voids (1–30 μm diameter) were intermittently observed at other locations by SEM (Fig. 7).

The microstructure of the α-Al_2O_3 scale on LS (Ni,Pt)Al was significantly different than that on LS NiAl. The oxide scale on (Ni,Pt)Al was measurably thicker (1–2.5 μm), and consisted of two discrete layers, as shown in Fig. 11b. The outer layer was approximately 1.2 μm thick and consisted of large-grain (~1.3 μm diameter) α-Al_2O_3 (determined by electron diffraction), containing numerous small (<0.3 μm) internal voids, very similar to the scale on NiAl. The inner layer of α-Al_2O_3 was approximately 1.0 μm thick with a finer grain size (~0.6 μm diameter), a columnar-type grain structure, and very few internal voids (Fig. 11b).

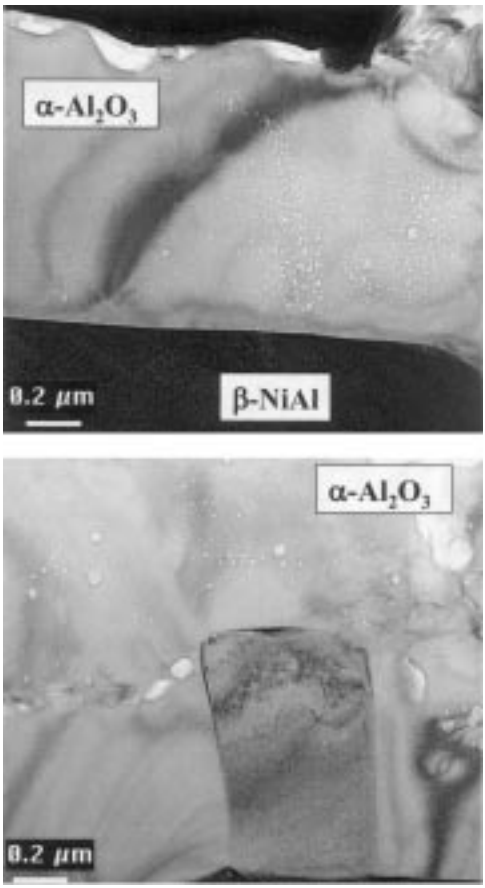

Fig. 11. TEM images of alumina scales on (a) LS NiAl and (b) LS (Ni,Pt)Al after 100 hr isothermal oxidation at 1150C. Note that the scale in (a) is thinner and more porous. The scale on (b) has a porous outer layer, similar to (a), and a dense, columnar-grain inner layer. The grain boundaries of the dense, inner region of (b) contained detectable levels of Hf by STEM.

Microchemical characterization by STEM/EDS confirmed the presence of Hf (from the superalloy) along the columnar grain boundaries of the inner layer of scale on LS (Ni,Pt)Al after 100-hr oxidation, as shown by the EDS map in Fig. 12a. Segregation of reactive elements, such as Zr and Y, to alumina-scale grain boundaries has been previously observed on cast NiAl.[22,44] Hafnium was not detected in the larger-grain, porous Al_2O_3 on

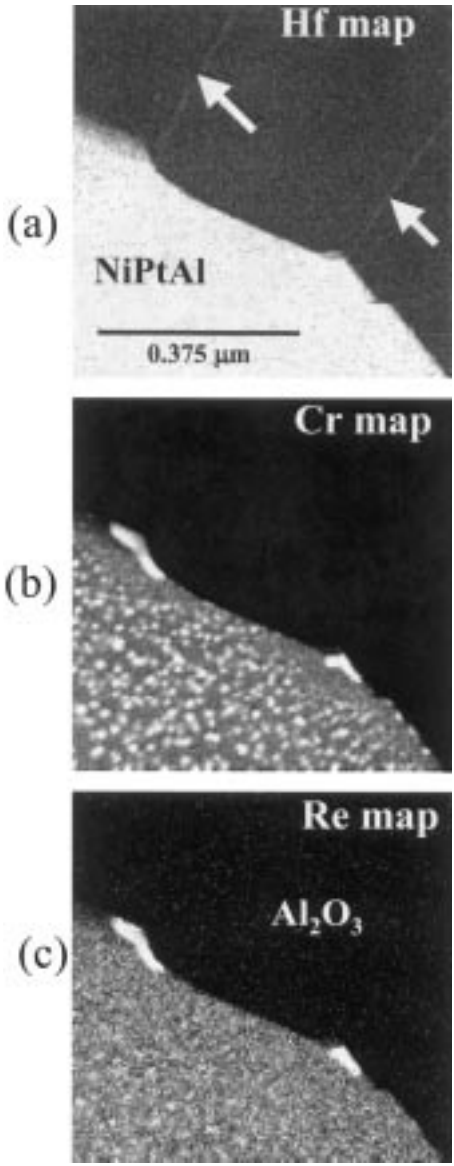

Fig. 12. STEM EDS maps of oxide–metal interface on LS (Ni,Pt)Al specimen in Fig. 11b after 200 hr at 1150°C. Note that the alumina grain boundaries in (a) contain Hf (arrows). Figures (b) and (c) show α-Cr particles rich in Re at both the oxide–metal interface and in the B2 matrix.

the outer surface of the scale. Identical mapping of the scale on LS NiAl after 100 hr did not detect Hf within the Al_2O_3 grains, grain boundaries, or at the oxide–metal interface (which does not necessarily mean that no Hf was present). Mapping also revealed the presence of spherical α-Cr particles within the β-(Ni,Pt)Al matrix and larger irregular-shaped α-Cr particles along the oxide–metal interface (Fig. 12b), as reported previously.[23] These Cr–rich particles also contained high concentrations of Re (Fig. 12c), with lesser amounts of Co and Mo. Similar α-Cr particles were also observed within the oxidized CVD NiAl and have been observed on cast NiAl + Cr + Hf.[41]

DISCUSSION

The results of this investigation indicate that minor amounts of substrate impurities and/or reactive elements can have a major effect on alumina-scale adherence and growth on aluminide coatings. Sulfur strongly influenced oxide adherence to and void growth on simple aluminide coatings. Platinum-modified aluminide coatings and castings showed excellent scale adherence and were not sensitive to sulfur impurities. Hafnium from the substrate was incorporated into some oxide scales and there were apparent differences in Hf diffusion from the substrate through the NiAl and (Ni,Pt)Al coatings. These results provide significant insight into potential mechanisms by which S, Pt, and Hf influence the microstructure and adherence of the Al_2O_3 scales that form on aluminide bond coatings.

Influences of Sulfur and Reactive Elements on Superalloys

It is generally agreed that S impurities degrade the adherence of protective oxide scales.[16–19] Sulfur is a surface-active element that is well known to segregate to surfaces and interfaces in metals. Although the exact mechanism by which S reduces scale adherence is still unclear, it likely involves increased formation of voids at the metal–oxide interface and/or weakening of the metal–oxide bond.

It is also generally agreed that appropriate additions of REs such as Hf, Y or Zr counter the detrimental role of S, possibly by one of the following mechanisms: (a) gettering of S from the matrix through the formation of stable reactive-element sulfides, presumably in the melt,[17,20,35] or (b) preferentially segregating to available sites or surfaces along the oxide–metal interface as a result of the reactivity and large ion size of REs, thus inhibiting segregation of embrittling S impurities to the interface region.[22] The presence of appropriate amounts of RE also reduces or prevents void formation at the oxide–metal interface of cast intermetallics.[22,35] It has been

suggested[35] there is some critical ratio of RE to S, and possibly C in the case of Hf,[26] that results in enhanced-scale adherence.

The detrimental influence of S was clearly illustrated by the oxidation behavior of the non-coated Y-free substrate superalloys in Fig. 2. The poor scale adherence to the HS bare superalloy (~7.0 ppma S) demonstrates that Hf in the superalloy was not sufficient to produce good scale adherence.[28] This result was expected from the previous observation that Hf in cast NiCrAl and FeCrAl is less effective than Y, except when S is very low.[45] Also, the relative atomic amount of Hf (~600 ppma), as compared to C and S (4885 and 7.0 ppma, respectively) in the HS alloy, suggests that most of the Hf may have been bound as stable carbides.[26]

The good scale adherence to the melt desulfurized alloy (Fig. 2) demonstrates the effectiveness of reducing S impurities. Both the HS and LS alloys in Fig. 2 had similar C contents (Table I), demonstrating that little decarburization occurs during melt de-sulfurizing, in contrast with the H_2 desulfurization process, which removes both C and S.[26,28,46] Thus, the superior scale adherence could not be attributed to a higher Hf activity, due to C removal,[26] and was most likely the result of S removal.

Influences of S, Pt, and Hf on Bond Coatings

The oxidation behavior of the CVD NiAl in this study (Fig. 3) confirmed the previous finding by Lee *et al.*[19] that scale adherence to simple aluminide coatings is very sensitive to S impurities resulting from processing and from the substrate. The very poor scale adherence to HS NiAl (Fig. 8) and the good performance of LS NiAl (Fig. 3) clearly demonstrate the detrimental effects of substrate S.

Perhaps the most important result of this study was the observation that oxide-scale adherence to the Pt-modified coatings exhibited no sensitivity to variations in substrate S impurities, at least within the range of substrate S (1.0–7.0 ppma) that was studied. Our previous work had suggested that Pt-modified coatings were not sensitive to S, but only low-sulfur substrates were used in that study.[14] Note that the (Ni,Pt)Al on both HS and LS substrates actually contained even greater amounts of S impurities than the NiAl, due to significant S contamination of the electroplated Pt.[14]

It is interesting to note that although the initial scale microstructure that formed on LS (Ni,Pt)Al was similar to that on LS NiAl (upper portions of Figs. 11a and b), the presence of Hf from the substrate appeared to eventually alter the scale-growth mechanism on (Ni,Pt)Al. The outer, non-doped layer of Al_2O_3 most likely formed via transformation of metastable θ-Al_2O_3 to α-Al_2O_3, resulting in a large-grain, equiaxed, porous microstructure (the pores formed due to a volume reduction during the transformation

from θ to α).[41] In the case of simple aluminides, these large Al_2O_3 grains continued to grow resulting in a slower growth rate due to the limited number of rapid transport paths. In the case of (Ni,Pt)Al, it appears that finer columnar grains nucleated beneath the equiaxed grains. Columnar grains suggest an inward growth mechanism and with more transport paths the scale would grow more quickly. It is not clear why Hf was detected on the oxide-scale grain boundaries of (Ni,Pt)Al, but was not detected on NiAl. One possibility is that sufficient quantities of Hf did not diffuse through the LS NiAl to enable the nucleation of finer, columnar grains. This observation suggests that the presence of Pt in the B2 structure may have altered the solubility and/or diffusion behavior of elements with large ion size, such as Hf, and possibly even S. The slower growth rate of Al_2O_3 on CVD NiAl (Table III) may be the result of fewer oxide grain boundaries due to the larger Al_2O_3 grain size.

It must also be considered that the superior scale adherence and resistance to void growth of CVD (Ni,Pt)Al may not have been solely due to the presence of Pt, since there was also a contribution of Hf. However, although numerous small internal voids were present in the first layer of scale on (Ni,Pt)Al, there was no evidence by TEM or SEM that significant growth of voids occurred at the metal–oxide interface prior to the arrival of sufficient Hf to dope the oxide grain boundaries (Fig. 11b). This suggests that although Pt did not prevent void nucleation it was effective to suppress void growth even without the presence of a significant amount of Hf. This observation is supported by prior research showing that the addition of Pt to cast alloys, with no RE addition, is an effective method of improving scale adherence,[9,10,31] although neither the scale-growth mechanism nor growth rate are affected.[31] These results were further confirmed by the behavior of the cast (Ni,Pt)Al alloys in this study, although the simultaneous addition of both Pt and Hf resulted in a greater improvement than just the addition of Pt, because of the added benefit of a significant reduction in scale growth rate (Fig. 3b).

The magnitude of comparative benefit of Hf and Pt within a coating still is not clear, but further work is being conducted. It is important to realize that the presence of Hf within the oxide scale on a coating means that it is difficult to effectively design or adequately compare oxidation studies of aluminide coatings without detailed knowledge of the actual superalloy composition, which can vary substantially from source to source or even batch to batch of the same nominal alloy. Furthermore, the effectiveness of Hf doping has been shown to be dependent on the relative C and S levels in NiAl.[47] These observations strongly suggest that future careful and systematic studies of high-temperature bond coat oxidation behavior clearly measure and define the C, Hf, Y, Zr, and S contents of each superalloy substrate batch.

Void Growth

Further insight into the mechanisms by which Pt improves scale adherence is provided by comparison of void growth behavior on CVD NiAl and (Ni,Pt)Al during isothermal oxidation, especially with respect to substrate S content. Our previous work attributed the dissimilarities in Al_2O_3 scale adherence on NiAl and (Ni,Pt)Al to differences in their tendency to form voids at the oxide–metal interface.[13,15,23] The present study further confirmed this conclusion, as LS NiAl formed small quantities of large voids (Figs. 6a and 7) but HS (Ni,Pt)Al formed no observable voids (Fig. 10).

The presence of voids on a substoichiometric NiAl coating with substrate sulfur of 1.0 ppma is consistent with the observations of Sarioglu and co-workers,[35] who observed voids (and in some cases trenches) on the grain boundaries of cast H_2-desulfurized (~0.1 ppma S) Ni–50Al (at.%) oxidized at 1100°C. They found numerous voids on grain boundaries and surfaces of the same alloy with 20 ppma S, but there were very few voids on the grain surfaces after desulfurization. Their study suggested a critical S content for void formation on cast NiAl at 1100°C of ~0.05 ppma, which is significantly less than the measured S levels of the LS substrates or LS NiAl in this study.

The significant increase in the number of voids on HS NiAl, as compared to LS NiAl, strongly suggests that impurities, most likely S, directly influence void growth in these hypostoichiometric coatings with Al contents of ~32 at.% after oxidation.[15] This appears to be especially true on the coating grain bodies (Fig. 8), where the number of voids increased dramatically as the atomic percentage of S increased by a factor of 7. The formation of greater numbers of more shallow voids on the HS CVD NiAl suggests an influence of impurities on both the nucleation and growth of stable voids. The differences in the amounts of voids cannot be attributed to dissimilarities in Al content, contrary to Brumm and Grabke,[29] since both the HS and LS NiAl coatings were essentially identical in Al and Ni contents. Furthermore, the total volume of voids at the oxide–metal interface in cross section appeared to be of the same order of magnitude for both types of coatings, since the LS coatings typically formed intermittent, deeper voids, whereas similar diameter voids on HS NiAl were typically more shallow. The similarity in the total volume of voids, regardless of substrate S content, suggests the possibility that excess vacancies may play a significant role in void nucleation and/or growth.

A Simple Vacancy-Related Model of the Sulfur Effect on Void Growth

A simple model of the S effect on void growth at the oxide–metal interface of hypostoichiometric β-NiAl coatings at 1150°C is proposed (Fig.

13) based on the observations of this study. Figure 13a shows a schematic cross section of a LS NiAl coating (with no reactive element) forming an Al_2O_3 scale. This model assumes that very fine perturbation voids[43] continuously form along the oxide–metal interface, with a higher probability that larger perturbation voids will form over discontinuities or interface perturbations, such as a coating grain boundary.[35,36,43] Similar-sized voids may also form within the scale and at the interface due to Al_2O_3 phase transformations.[41,43] Inward growth of the scale by consumption of Al results in encapsulation of most of the very fine interface voids within the Al_2O_3.[43] However, some of the interfacial perturbation voids may reach a critical size and continue to grow into the NiAl instead of being encapsulated in the scale. The relatively small number of visible voids on LS NiAl coatings suggests that only a few perturbation voids, most of them on the coating grain boundaries, exceeded a critical size (Fig. 7).

Several diffusion-related processes may contribute to stabilization and growth of voids on LS NiAl (Fig. 7), as illustrated by the schematic in Fig. 13b. First, S impurities may stabilize perturbation voids by segregating from the coating matrix to the void surface,[37] and possibly the metal–oxide interface,[48,49] in order to lower the system free energy. These sulfur-stabilized voids would have a higher probability of achieving critical size. Second, the presence of such a critical-sized void would make it energetically favorable for the void to continue to grow by transport and coalescence of excess vacancies from the surrounding NiAl matrix (i.e., the void would serve as a vacancy sink). The interfacial void may specifically serve as a sink for excess vacancies injected into the metal by outward diffusion of cations into the oxide scale[42,50,51] or those due to unequal fluxes of Al and Ni/Pt throughout the Al-deficient aluminide coating or by more rapid diffusion of Ni away from the void[52] as Al diffuses to the surface (Fig. 7c). Increases in equilibrium vacancy concentration as the Al content is decreased[52] during oxidation could provide a primary driving force for continued vacancy condensation and void growth.[38] Void growth may be further facilitated by vaporization of Al from the void surface.[42,53] In a β-NiAl structure, with low S concentration, void growth would be most prevalent over the coating grain boundaries, where there would be more rapid transport of S, Al, and vacancies to the surface, as well as Ni away from the void surface.

Based on this very simple model, at a constant oxidation temperature, one would expect several changes in void growth to occur if the S concentration increased significantly, with the Al and Ni concentrations remaining approximately the same. First, greater quantities of S might be available to segregate from the coating matrix to the metal–oxide interface, in addition to the coating grain boundaries, so that voids should be more numerous on grain bodies, as suggested in Fig. 13c. This assumption agrees with the

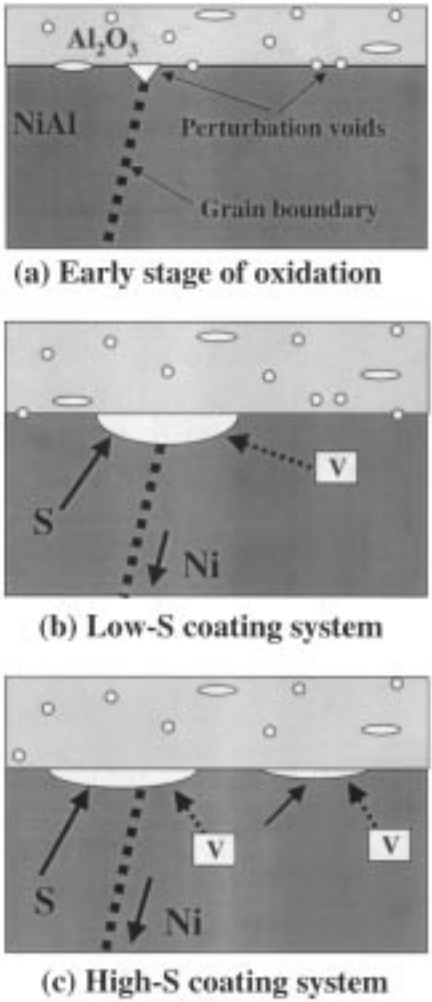

Fig. 13. Simple model of S influence on void growth. (a) Early stage of oxidation. Perturbation voids are encapsulated within the growing scale. Largest voids form over grain boundaries. (b) Low-S coating. Voids stabilized by S act as a vacancy sink and grow over grain boundaries. Rapid back-diffusion of Ni contributes to rapid void growth over grain boundaries. (c) High-S coating. More voids form, with voids also forming on grain surfaces due to greater and more rapid availability of S. Voids are more shallow due to greater numbers and a relatively constant volume of excess vacancies.

Table IV. Measured Void Dimensions after 200 hr Isothermal Oxidation at 1150°C

Specimen	Mean void diameter (μm)	Min./max. void diameter (μm)	Mean void depth (μm)	Min./max. void depth (μm)
LS NiAl	16.3 ± 5.9	7.5–25	5.5 ± 2.9	1.4–9.2
HS NiAl	21.3 ± 13	3.7–67	4.4 ± 2.0	0.7–7.9

results shown in Fig. 8. Second, greater quantities of voids would also grow over the grain boundaries due to the even greater and more rapid availability of S to stabilize more perturbation voids. The numerous, rapid-growing grain-boundary voids could be expected to eventually coalesce and form "trenches" around some grains, as occurred on the HS NiAl in this study (Fig. 8). Third, if the concentration of excess vacancies at 1150°C is constant in the β-NiAl matrix (i.e, no influence of S on vacancy generation and no significant difference in oxide growth rate at these S levels), then it is possible that the total volume of voids generated per unit volume of intermetallic would be similar regardless of coating S content. However, the volume of voids would not necessarily be identical since there could also be internal vacancy sinks such as coating grain boundaries. In the case of a higher-S coating, since more voids would grow to exceed the critical size for stability, the average volume of metal displaced by each individual void should be smaller. This should result in greater numbers of voids with either smaller diameter or more shallow depth of penetration into the NiAl. In fact, large-diameter voids would likely be the result of coalescence of several closely spaced smaller voids and as such should have a relatively shallow depth of penetration into the coating. This behavior is generally consistent with that observed on the HS NiAl coatings of this study (Table IV).

The Influence of Pt on Void Growth

Void growth at the metal–oxide interface on aluminide castings and coatings is significantly reduced or eliminated when Pt is present, although the mechanism is not clear. Void growth is also eliminated or reduced by reactive-element additions. However, the Pt effect is clearly different than the REE, since 0.05 at.% Hf is required while ~5 at.% Pt is necessary and Pt does not reduce scale-growth rates like a reactive element. Extending the previously discussed model (Fig. 13) to consider this question suggests several possibilities by which the presence of Pt, in solid solution within the B2 matrix, may benefit scale adherence. Platinum could modify (probably reduce) the equilibrium concentration or transport rate of thermal vacancies at 1150°C. This might serve to reduce the driving force for void nucleation,

especially if there is a vacancy threshold above which interfacial voids readily form. It is also possible that the presence of Pt in solid solution strengthens bonding at the metal–oxide interface, which might suppress or prevent growth of voids. The presence of Pt on the Ni sites in the B2 lattice may also alter the tendency to form Ni antisite defects as the Al concentration decreases during oxidation,[52] thus decreasing the total vacancy content of the system. Recent observations that voids form on Hf-free, Pt-modified alumindes in the presence of very high substrate sulfur (i.e., >15 ppma) levels[55] show that the beneficial effect of Pt can be overwhelmed if sufficient sulfur is present. Platinum aluminides will also form voids after prolonged cyclic oxidation at 1150°C, as shown in this (Fig. 5b) and other studies.[56] These limits suggest that the Pt effect may also involve modification of S solubility,[55] diffusion and/or segregation. The possibility that the presence of Pt alters the generation or mobility of vacancies in Ni-rich intermetallics is currently being explored via thermal expansion studies.[7]

An alternative explanation of the influence of Pt is that the combination of a stronger metal–oxide interface and the presence of Kirkendall-type voids at the coating–superalloy interface within the (Ni,Pt)Al may preferentially accommodate both excess vacancies and S within internal defects, instead of at the oxide–metal interface. However, such a mechanism would not account for the excellent scale adherence on cast Pt-modified alloys.[56] While the actual mechanism(s) remain the subject of speculation, it is clear that one of the major benefits of Pt is to significantly reduce the driving force for void growth at the metal–oxide interface. In this regard, while the results of this study have provided significant insight into the detrimental role of S on scale adherence, identification of the mechanism(s) of the Pt effect will require further investigation.

SUMMARY

1. The cyclic oxidation behavior of ultrahigh-purity CVD NiAl coatings at 1150°C was sensitive to substrate S impurities. Reductions in S impurities resulted in dramatic improvements in scale adherence.

2. Scale adherence to CVD (Ni,Pt)Al coatings at 1150°C was not sensitive to substrate S impurities, within the S concentrations (1.0–7.0 ppma) of this study.

3. Void growth along the Al_2O_3–NiAl interface during isothermal oxidation at 1150°C was very sensitive to substrate S impurities. The number of voids on the coating surface increased significantly as substrate S increased from 1.0 to 7.0 ppma, although voids were typically more shallow on the higher-S coating.

4. Voids did not form at the oxide–metal interface of CVD (Ni,Pt)Al with higher substrate S (7.0 ppma).

5. Significant differences in the microstructures of the alumina scales formed on NiAl and (Ni,Pt)Al were revealed by TEM. Columnar-grain scales on (Ni,Pt)Al were doped with Hf, whereas Hf was not detected in scales on NiAl.

6. A simple vacancy-related model was proposed to explain the influence of S on void growth within NiAl coatings.

ACKNOWLEDGMENTS

The authors thank C. Kortovich and L. Graham of PCC Airfoils for providing superalloy substrate material; B. Warnes and N. DuShane of Howmet Corporation for conducting Pt electroplating; L. D. Chitwood and G. Garner at ORNL for assisting with oxidation experiments; Tom Geer, Dorothy Coffee, and L. Walker at ORNL for metallography, FIB–TEM specimen preparation, and EPMA analysis. Thanks to K. Putyera at Shiva Technologies (Syracuse, NY) for GDMS. The authors also thank Ted Besmann, Pete Tortorelli, and Mike Brady at ORNL for reviewing the manuscript. This research was sponsored by the Advanced Gas Turbine Systems Program, DOE Office of Industrial Technologies, under contract DE-AC05–96OR22464 with UT-Batelle Limited Liability Corporation.

REFERENCES

1. A. Maricocchi, A. Bartz, and D. Wortman, *J. Thermal Spray Technol.* **6**(2), 193 (1997).
2. M. Gell, K. Vaidyanathan, B. Barber, J. Cheng, and E. Jordan, *Met. Trans. A* **30A**, 427 (1999).
3. S. M. Meier, D. K. Gupta, and K. D. Sheffler, *JOM* **43**, 50 (1991).
4. W. P. Parks, E. E. Hoffman, W. Y. Lee, and I. G. Wright, *J. Thermal Spray Technol.* **6**(2), 187 (1997).
5. P. K. Wright, *Mater. Sci. Eng.* **A245**, 121 (1998).
6. D. V. Rigney, R. Viguie, D. J. Wortman, and D. W. Skelly, *J. Thermal Spray Technol.* **6**(2), 167 (1997).
7. J. A. Haynes, B. A. Pint, W. D. Porter, and I. G. Wright, *Mater. High Temp.*, submitted (2001).
8. G. Lehnert and H. Meinhardt, *Electrodep. Surf. Treat.* **1**, 189 (1973).
9. E. J. Felten, *Oxid. Met.* **10**, 23 (1976).
10. E. J. Felten and F. S. Pettit, *Oxid. Met.* **10**, 189 (1976).
11. J. S. Smith and D. H. Boone, *ASME Paper No. 90-GT-319* (American Society of Mechanical Engineers, New York, 1990).
12. M. S. Farrell, D. H. Boone, and R. Streiff, *Surf. Coat. Technol.* **32**, 69 (1987).
13. J. A. Haynes, Y. Zhang, W. Y. Lee, B. A. Pint, I. G. Wright, and K. M. Cooley, in *Elevated Temperature Coatings: Science and Technology III*, J. M. Hampikian and N. B. Dahotre, eds. (The Minerals, Metals and Materials Society, 1999), pp. 185–196.
14. Y. Zhang, W. Y. Lee, J. A. Haynes, I. G. Wright, B. A. Pint, K. M. Cooley, and P. K. Liaw, *Metall. Trans. A* **30A**, 2679 (1999).

15. Y. Zhang, J. A. Haynes, W. Y. Lee, I. G. Wright, B. A. Pint, K. M. Cooley, and P.K. Liaw, *Metall. Mater. Trans. A* **32**(7), 1727 (2001).
16. J. G. Smeggil, *Mater. Sci. Eng.* **87**, 261 (1987).
17. J. L. Smialek, *Metall. Trans. A* **18A**, 164 (1987).
18. J. L. Smialek, D. T. Jayne, J. C. Schaeffer, and W. H. Murphy, *Thin Solid Films* **253**(1), 285 (1994).
19. W. Y. Lee, Y. Zhang, I. G. Wright, B. A. Pint, and P. K. Liaw, *Metall. Trans. A* **29A**, 833 (1998).
20. J. G. Smeggil, A. W. Funkenbusch, and N. S. Bornstein, *Metall. Trans. A* **17A**, 923 (1986).
21. A. Strawbridge and P. Y. Hou, *Mater. High Temps.* **12**, 177 (1994).
22. B. A. Pint, *Oxid. Met.* **45**, 1 (1996).
23. J. A. Haynes, K. L. More, B. A. Pint, I. G. Wright, K. Cooley, and Y. Zhang, *Mater. Sci. Forum* **369–372**, 679 (2001).
24. W. C. Basta, D. C. Punola, and B. M. Warnes, US Patent 5,658,614 (1997).
25. B. M. Warnes and D. C. Punola, *Surf. Coat. Technol.* **94–95**, 1 (1997).
26. I. G. Wright, B. A. Pint, W. Y. Lee, K. B. Alexander, and K. Prüßner, in *High-Temperature Surface Engineering*, *Institute of Materials*, J. Nicholls and D. Rickerby, eds., Book 693 (IOM Communications Ltd., 2000), pp. 95–113.
27. K. L. More, D. W. Coffey, B. A. Pint, K. S. Trent, and P. F. Tortorelli, *Proc. Microsc. Microanalysis 2000*, **6**(2), 540 (2000).
28. J. L. Smialek and B. A. Pint, *Mater. Sci. Forum* **369–372**, 459 (2001).
29. M. W. Brumm and H. J. Grabke, *Corros. Sci.* **34**, 547 (1993).
30. B. A. Pint, *Oxid. Met.* **49**, 531 (1998).
31. B. A. Pint, I. G. Wright, W. Y. Lee, Y. Zhang, K. Prüßner, and K. B. Alexander, *Mater. Sci. Eng. A* **A245**, 201 (1998).
32. M. W. Brumm and H. J. Grabke, *Corros. Sci.* **33**, 1677 (1992).
33. J. L. Smialek, in *Microscopy of Oxidation 3*, *Proceedings of the Third International Conference on the Microscopy of Oxidation*, S. B. Newcomb and J. A. Little, eds. (Institute of Materials, London, 1996), pp. 127–139.
34. K. Prüßner, E. Schumann, and M. Rühle, in *Fundamental Aspects of High Temperature Corrosion*, Vol. 96-26, D. A. Shores, R. A. Rapp, and P. Y. Hou, eds. (The Electrochemical Society, Pennington, NJ, 1997), pp. 344–356.
35. C. Sarioglu, C. Stinner, J. R. Blachere, N. Birks, F. S. Pettit, G. H. Meier, and J. L. Smialek, in *Superalloys 1996*, R. D. Kissinger, D. J. Deye, D. L. Anton, A. D. Cetel, M. V. Nathal, T. M. Pollock, and D. A. Woodford, eds. (TMS, Warrendale, PA, 1996), pp. 71–80.
36. A. Katsman, H. J. Grabke, and L. Levin, *Oxid. Met.* **46**, 313 (1996).
37. H. J. Grabke, G. Kurbatov, and H. J. Schmutzler, *Oxid. Met.* **43**, 97 (1995).
38. D. Oquab and D. Monceau, *Scripta Mater.* **44**, 2741 (2001).
39. J. Doychak, J. L. Smialek, and C. A. Barrett, *Oxidation of High-Temperature Intermetallics*, T. Grobstein and J. Doychak, eds. (TMS, Warrendale, PA, 1988), pp. 41–56.
40. V. K. Tolpygo and D. R. Clarke, *Mater. High. Temp.* **17**, 59–70 (2000).
41. B. A. Pint, K. L. More, I. G. Wright, and P. F. Tortorelli, *Mater. High Temps.* **17,** 165 (2000).
42. H. M. Hindam and W. W. Smeltzer, *J. Electrochem. Soc.*, pp. 1630–1635 (1980).
43. B. A. Pint, *Oxid. Met.* **48**, 303 (1997).
44. E. Schumann, J. C. Yang, M. Rühle, and M. J. Graham, *Oxid. Met.* **46**, 37 (1996).
45. B. A. Pint and I. G. Wright, unpublished research (2001).
46. J. L. Smialek, *Oxid. Met.* **55**, 75 (2001).
47. I. G. Wright and B. A. Pint, *Proc. SF2M 2000: Journées d'automne*, *Société Française de Métallurgie et de Matériaux*, (Paris), pp. 86–96 (2000).
48. P. Y. Hou, K. Prüßner, D. H. Fairbrother, J. G. Roberts, and K. B. Alexander, *Scripta Mater.* **40**, 241 (1999).
49. V. K. Tolpygo and H. Viefhaus, *Oxid. Met.* **52,** 1 (1999).
50. R. Hutchings, M. H. Loretto and R. E. Smallman, *Metal Sci.*, **15,** 7 (1981).
51. G. B. Gibbs and R. Hales, *Corros. Sci.* **17**, 487 (1977).

52. M. P. Gururajan and T. A. Abinandanan, *Intermetallics*, **8**, 759 (2000).
53. Homma, H. M. Hindam, Y. Pyun, and W. W. Smeltzer, *Oxid. Met*. **17**, 223 (1982).
54. J. K. Tien and F. S. Pettit, *Metall. Trans*. **3**, 1587 (1972).
55. J. A. Haynes, *Scripta. Mater*. **44**, 1147 (2001).
56. E. C. Dickey, B. A. Pint, K. B. Alexander, and I. G. Wright, *J. Mater. Res*. **14,** 4531 (1999).